

Enhanced Thermoelectric Performance in Hybrid Nanoparticle–Single Molecule Junctions

Elinor Zerah-Harush¹ and Yonatan Dubi^{1,2*}

¹*Department of Chemistry and* ²*Ilse-Katz Institute for Nanoscale Science and Technology,
Ben-Gurion University of the Negev, Beer-Sheva 84105, Israel*

(Dated: April 18, 2017)

It was recently suggested that molecular junctions would be excellent elements for efficient and high-power thermoelectric energy conversion devices. However, experimental measurements of thermoelectric conversion in molecular junctions have indicated rather poor efficiency, raising the question of whether it is indeed possible to design a setup for molecular junctions that will exhibit enhanced thermoelectric performance. Here we suggest that hybrid single-molecule nanoparticle junctions can serve as efficient thermoelectric converters. The introduction of a semiconducting nanoparticle introduces new tuning capabilities, which are absent in conventional metal-molecule-metal junctions. Using a generic model for the molecule and nanoparticle with realistic parameters, we demonstrate that the thermopower can be of the order of hundreds of microvolts per degree Kelvin, and that the thermoelectric figure of merit can reach values close to one, an improvement of four orders of magnitude improvement over existing measurements. This favorable performance persists over a wide range of experimentally relevant parameters, and is robust against disorder (in the form of surface-attached molecules) and against electron decoherence at the nanoparticle molecule interface.

INTRODUCTION

In recent years, the study of single-molecule junctions – the ultimate limit of electronic nano-technology – has progressed well beyond their role as functional elements in electronic devices [1], and today additional functionalities, from opto-electronics and spintronics, through phononics, to thermoelectricity [2–4] are under investigation. The potential applicability of single-molecule junctions in thermoelectricity – the conversion of heat into electric power – is of particular interest, since thermoelectricity may turn out to be an important element in addressing global energy issues [5, 6]. The clear advantages of thermoelectric energy conversion, such as the “green” nature of the energy conversion process, its applicability for waste heat harvesting, and the easy device maintenance due to the absence of moving parts, would lead us to think that thermoelectric devices should already be a substantial part of the energy market, yet this is not the case. The reason lies in the simple fact that current thermoelectric devices are not efficient enough, making competition with traditional (large scale) energy conversion systems virtually impossible.

Due to their versatility, low dimensionality, and low thermal conductivity, molecular junctions offer a possible route for enhancing thermoelectric performance [7]. Indeed, various theoretical studies have suggested that molecular junctions could be a key component of efficient and high-power thermoelectric devices [8–16]. Experimental demonstrations [17–26], however, have indicated just the opposite, as can be deduced by examining the two central parameters of thermoelectric conversion, the thermopower (or the Seebeck coefficient) and the thermoelectric figure of merit (FOM).

The thermopower S measures the voltage generated per unit temperature difference (in the linear response) [4, 19, 27, 28]. Values of $S \sim 10^2 - 10^3 \mu\text{V/K}$ are typical for standard semi-conductor based thermoelectrics, yet molecular junctions exhibit small values of S , typically $S \sim 5 - 50 \mu\text{V/K}$. The FOM, namely ZT , defined as $ZT = \frac{GS^2}{\kappa/T}$, where G is the conductance of the junction, $\kappa = \kappa_e + \kappa_{phn}$ is the total thermal conductance, which includes both electronic (e) and phononic (phn) contributions, and T is the temperature. ZT is directly related to the device efficiency [29], and $ZT \rightarrow \infty$ corresponds to the Carnot efficiency (thus, theoretically, there is no upper bound on ZT). It is commonly held that, from the efficiency perspective, a ZT of ~ 4 is required for thermoelectric conversion to be competitive [30]. However, typical ZT values obtained from measurements in molecular junctions are $ZT \sim 10^{-3} - 10^{-5}$. Thus, there seems to be a discrepancy between theoretical and computational studies of thermoelectric conversion in molecular junctions, which in many cases [8–14] predict $S \sim 10^2 - 10^3 \mu\text{V/K}$ and FOM of $ZT \gg 1$, and the experimental evaluation of the two measures.

The origin of this discrepancy seems to stem from two factors. First, one has to be careful to take the phonon contribution to the thermal conductance into account; a typical and realistic value for the phonon thermal conductance in molecular junctions is $\kappa_{phn} = 10 - 100 \text{ pW/K}$ [13, 19, 31–33]. Second, many calculations show enhanced thermoelectric performance based on tuning of the molecular orbitals or, equivalently, the Fermi level of the electrodes. However, in reality this tuning is very difficult to achieve [24, 34–36], and the only “tuning parameter” available for molecular junctions is the choice of the molecular moiety. It is thus a central challenge to

design molecular junctions that are both tunable in some way and show favorable thermoelectric performance with realistic parameters.

In this paper, we present a new setup for molecular junctions that has the potential to achieve this goal. Our setup is based on a hybrid single-molecule semiconducting nanoparticle (SC-NP) structure in which a molecule is connected on one side to a metallic electrode (as in conventional molecular junctions), and on the other side connected to the second electrode through a SC-NP placed on the electrode, as is schematically depicted in Fig. 1(a). In this setup, the molecular junction can be tuned via tuning the electronic properties of the nanoparticle, namely, by choosing a suitable material and by controlling the size and shape of the nanoparticle (for reviews see, e.g., [37–39]). Fabrication of hybrid NP-single molecule junctions have already been demonstrated with Au NPs (see, e.g., [40–42]), making our suggested system experimentally feasible.

Using a generic model for the SC-NP, we show that this junction can reach values of $S \sim 100 - 400 \mu\text{V/K}$ and $ZT \sim 1$ for a broad range of realistic parameters. The origin of the enhanced thermoelectric performance can be traced to the interplay between the local transport properties of the molecule and the gapped density of states (DOS) of the nanoparticle [13]. Thermoelectricity typically requires a large particle-hole asymmetry (reflected in the fact that, at low temperatures, the thermopower is proportional to the derivative of the transmission function [4, 19, 28]). This asymmetry is enhanced in this junction due to the presence of the semiconducting gap in the SC-NP [13], an effect that is rectified due to the finite size of the nanoparticle. We show that the optimal parameters for thermoelectric conversion depend on the geometry of the nanoparticle and the contact geometry between the nanoparticle and the molecule. Further, we demonstrate that the favorable thermoelectric performance is robust against disorder (in the form of surface dangling molecules) and dephasing, and finally, we discuss the temperature dependence of the FOM, which exhibits a maximum at $T \sim 450 \text{ K}$.

MODEL AND CALCULATION

The transport and thermoelectric properties of the hybrid molecule-nanoparticle junction are calculated by using the non-equilibrium Green's function approach, which has become the standard tool for such calculations [27, 28]. The junction (graphically depicted in Fig. 1(a)) is described using the Hamiltonian:

$$\mathcal{H} = \mathcal{H}_B + \mathcal{H}_{NP} + \mathcal{H}_M + \mathcal{H}_T + \mathcal{H}_{B-NP} + \mathcal{H}_{NP-M} + \mathcal{H}_{M-T} , \quad (1)$$

that includes the bottom electrode (B), the nanoparticle (NP), the molecule (M), the top electrode (T), and the

coupling between the bottom electrode and nanoparticle (B-NP), between the NP and the molecule (NP-M) and between the molecule and the top electrode (M-T). Since electron spin does not play a role in the mechanisms we describe here for enhancement of thermoelectricity, we treat spinless electrons.

To describe the SC-NP, we use a generic tight-binding model for a semiconductor [43–48] of the form

$$\mathcal{H}_{NP} = \sum_{\mathbf{r}} (\epsilon_c + \frac{\Delta}{2} (-1)^{P_{\mathbf{r}}}) c_{\mathbf{r}}^{\dagger} c_{\mathbf{r}} - t \sum_{\langle \mathbf{r}\mathbf{r}' \rangle} c_{\mathbf{r}}^{\dagger} c_{\mathbf{r}'} , \quad (2)$$

where the summation is taken over the atom positions \mathbf{r} (assumed to form a cubic lattice); $c_{\mathbf{r}}^{\dagger}(c_{\mathbf{r}})$ creates (annihilates) an electron at position \mathbf{r} ; t is the nearest-neighbor hopping matrix element; ϵ_c is the position of the band-gap center; and Δ is the semiconductor band-gap. The function $P_{\mathbf{r}} = x + y + z$ gives a modulation of the on-site energy $\epsilon_c \pm \frac{\Delta}{2}$ between neighboring atoms, generating a gapped band at the thermodynamic limit [44]. We point that although *ab initio* methods for calculating properties of NPs are emerging [49, 50], these are still not developed for transport calculations. Furthermore, since we are aiming at presenting general properties of hybrid junctions, our tight-binding calculation is generic and not limited to a specific system.

The molecule is described as a single orbital, which can correspond to either the HOMO or LUMO, depending on the position of the orbital energy [28]. The molecular Hamiltonian is simply

$$\mathcal{H}_M = \epsilon_0 d^{\dagger} d , \quad (3)$$

where $d^{\dagger} (d)$ creates (annihilates) an electron at the molecular orbital. In addition to the calculations described below, we performed calculations that also include a Coulomb interaction term (for the molecule) and spin-full fermions (by using the equations-of-motion method [51, 52]) but found no quantitative change in the main results, and therefore we keep the description here as simple as possible and treat electrons as non-interacting particles. The coupling between the molecule and the nanoparticle is described by the Hamiltonian:

$$\mathcal{H}_{NP-M} = -t_1 c_{\mathbf{r}_M}^{\dagger} d + h.c. , \quad (4)$$

where \mathbf{r}_M is the position of the atom in the nanoparticle that is in contact with the molecule, and t_1 is the hopping matrix element related to the overlap integral between the molecular orbital and the atomic level at \mathbf{r}_M .

The metallic top and bottom electrodes are assumed to be non-interacting metals [53] with the Hamiltonian $\mathcal{H}_X = \sum_k \epsilon_k c_{k,X}^{\dagger} c_{k,X}$, $X = T, B$ [27, 28, 53]. The coupling between the molecule and the top electrode (representing, e.g., the tip of a scanning tunneling microscope) is represented by the Hamiltonian term

$\mathcal{H}_{M-T} = \sum_{k,T} V_{k,T} c_{k,T}^\dagger d + h.c.$. Similarly, the contact between the bottom electrode and the nanoparticle is described by $\mathcal{H}_{B-MP} = \sum_{\mathbf{r} \in B} V_{k,B} c_{k,B}^\dagger c_{\mathbf{r}} + h.c.$. To proceed with the transport calculations, the metallic electrodes are treated within a wide-band approximation [54] (valid since our model is for non-interacting electrodes), where the top electrode is defined by a (retarded and advanced) self-energy term $\Sigma_T^{r,a} = \mp i \frac{\Gamma_T}{2} |M\rangle\langle M|$, in which $|M\rangle$ is the single-particle molecular orbital, and Γ_T is the electrode-induced level broadening. Similarly, the bottom electrode is defined via the self-energy term $\Sigma_B^{r,a} = \mp i \frac{\Gamma_B}{2} \sum_{\mathbf{r} \in B} |\mathbf{r}\rangle\langle \mathbf{r}|$, where Γ_B is the broadening due to the bottom electrode and the summation is taken over all the atom positions in the nanoparticle that are in contact with the bottom electrode. We point that the model described above (and specifically the wide band approximation) implies electron-phonon-induced thermalization in the electrodes, but no electron-phonon interaction in the junction at this stage. All the relevant energies- the Fermi level of the electrodes, NP valence and conduction bands, and molecular orbitals - are schematically also shown in Fig. 1(a).

Once the Hamiltonian and the self-energies are defined, the calculation proceeds via the non-equilibrium Green's function approach, which is reduced to the Landauer formalism for non-interacting electrons. [27, 55, 56]. The Green's functions are determined via $G^{r,a} = (E - \mathcal{H} + \Sigma^{r,a})^{-1}$, where $\Sigma^{r,a} = \Sigma_T^{r,a} + \Sigma_B^{r,a}$. The transmission function is given by $T(E) = \text{Tr}(\Sigma_T^r G^r \Sigma_B^a G^a)$, and the transport coefficients, namely, the conductance G , the thermopower S , and the thermal conductance κ , are determined within the Landauer formalism as $G = e^2 L_0$, $S = L_1/(eTL_0)$, $\kappa = (L_2 - \frac{L_1^2}{L_0})/T$, where T is the temperature (room temperature, unless otherwise stated) and $L_n = -\frac{1}{h} \int dE T(E) (E - \mu)^n \frac{\partial f}{\partial E}$ are the Landauer integrals, with h being Planck's constant, μ the chemical potential of the electrodes, and $f(E)$ the Fermi-Dirac distributions. The thermoelectric FOM ZT is given by $ZT = \frac{GS^2}{\kappa/T}$.

RESULTS

We start by describing the thermopower S and FOM ZT for a single molecule placed on a square pyramid-shaped nanoparticle [57, 58] (the bottom electrode is in contact with the [111] plane), as shown in Fig. 1(a). Since we present here a generic model for nanoparticles, we are not aiming at obtaining quantitative results describing a specific system. We are, nonetheless, aware that it is essential to take numerical parameters that are realistic and readily describe experimental systems. We thus choose the semiconducting band center at $\epsilon_c = -4.8$ eV and $\Delta = 0.8$ eV, corresponding to PbSe nanoparticles, and $\mu = -5.1$ eV as the electrode chemical potential

(corresponding to Au electrodes). Other numerical parameters were $t = 1.6$ eV, $\Gamma_B = 0.05$ eV, $\Gamma_T = 0.01$ eV (describing weakly coupled molecules, see, e.g., [59]). The pyramid basis contains 10×10 atoms, and our results only weakly (and quantitatively) depend on the size of the nanoparticle.

In Fig. 1(b), we show the thermopower S as a function of molecular orbital energy level ϵ_0 and the molecule-nanoparticle coupling t_1 . In experiments, ϵ_0 can be tuned by choice of molecule and by choice of the nanoparticle composition and size. The coupling t_1 can be additionally tuned by stretching or squeezing the molecular junction with the top electrode [60–62]. As may be seen, S can reach values as high as ± 200 $\mu\text{V/K}$ and can change sign according to the position of the molecular level with respect to the semiconducting band edge.

The appearance of a thermopower maximum upon a change in ϵ_0 is not surprising, since one would expect that tuning ϵ_0 would lead to a near resonance in transmission (which implies a maximum thermopower). However, the appearance of a maximum upon a change of t_1 is surprising; in a typical single-molecule junction, stretching the junction will only lead to a change in the molecule-electrode coupling, and will not result in a thermopower maximum. Here, since the molecule and the NP hybridize, changing t_1 (experimentally - by means of pulling the junction) is similar to changing the molecular orbital, i.e. pulling the junction plays the role of gating. Since gating a molecular junction is a challenging task [24, 34–36], this result puts an additional advantage on hybrid junctions.

To calculate ZT , we add to the electronic thermal conductance a phononic term $\kappa_{phn} = 50$ pW/K, a realistic value for molecular junctions [19, 31–33]. In Fig. 2, we plot the central result of this paper, ZT of the hybrid single-molecule-NP junction, as a function of ϵ_0 and t_1 . The FOM reaches $ZT > 0.8$, i.e., more than three orders of magnitude larger than the values measured in regular molecular junctions. The realistic parameters considered here and the wide range of parameters in which ZT is large implies that this regime should be accessible for experiments.

In the inset of Fig. 2, we show ZT as a function of ϵ_0 for a constant $t_1 = 0.1$ eV for three different configurations. The first (solid blue line) is the same as the setup in the main figure. In the second setup (dotted orange line), the molecule is in contact with a pyramid nanoparticle, but the positions of the $\pm\Delta$ terms in the nanoparticle Hamiltonian of Eq. 2 are switched, modeling a change in the atom species at the apex of the nanoparticle (for instance either Pb or Se in PbSe nanoparticles). The third setup (dashed green line) describes a molecule in contact with a cube-shaped (as opposed to a pyramid) nanoparticle. As may be seen, the contact configuration and the shape of the nanoparticle can have a strong effect on ZT ; although values of $ZT > 0.8$ can be achieved in these configura-

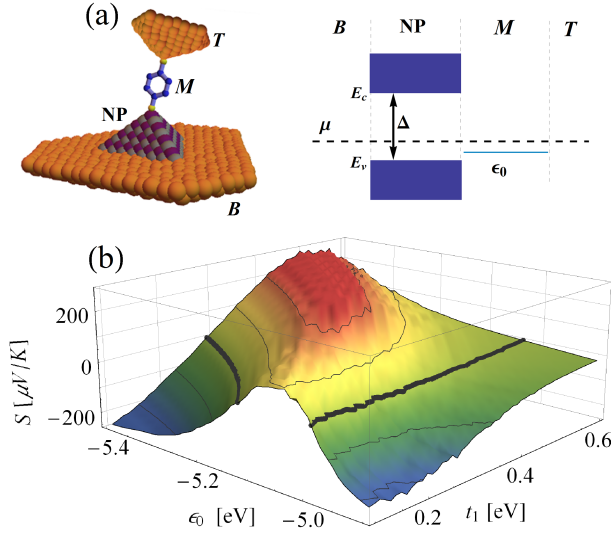


FIG. 1. (a) Schematic representation of the hybrid metal-molecule-nanoparticle-metal junctions (the choice of molecule is arbitrary), and the corresponding energy landscape. (b) Thermopower S as a function of the position of the molecular orbital ϵ_0 and molecule-nanoparticle coupling t_1 for a hybrid molecular junction with a square-pyramid-shape (see text for numerical parameters).

tions, the optimal parameters vary between the different setups.

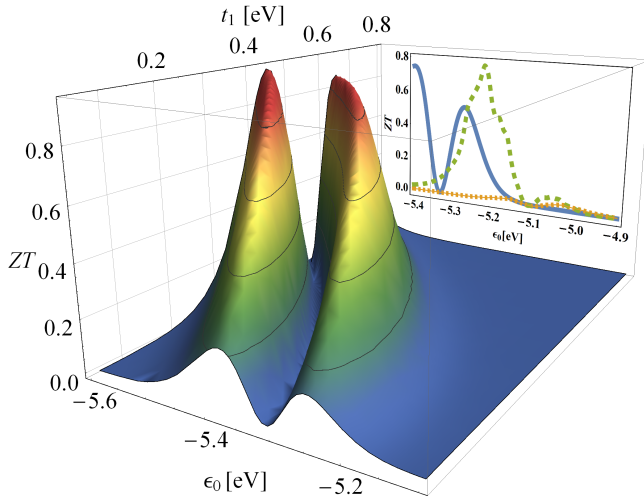


FIG. 2. ZT as a function of the position of the molecular orbital ϵ_0 and the molecule-nanoparticle coupling t_1 for a hybrid molecular junction with a square-pyramid shape (see text for numerical parameters). Inset: ZT as a function of ϵ_0 for a constant $t_1 = 0.1$ eV, for the hybrid junction with a pyramid nanoparticle (blue solid line), a pyramid nanoparticle with switched $\pm\Delta$ positions (dotted orange line, see text), and a cube-shaped nanoparticle (dashed green line).

In experiments, a reasonable situation would be for ad-

ditional molecules to attach to the surface of the nanoparticle. To model this scenario, we add to the Hamiltonian additional molecules, with the same orbital level ϵ_0 and coupling t_1 but with a random coupling point to the surface of the nanoparticle (top inset in Fig. 3). The transport properties are then averaged over 10^4 realizations of random positions. In Fig. 3, ZT is plotted as a function of surface coverage (in percents) of attached molecules. Surprisingly, we found a slight increase of ZT for a small number ($\sim 8\%$) of attached molecules, followed by a decrease in ZT when the number of attached molecules was increased. To elucidate the origin of this result, the lower inset shows the average conductance (blue circles) and thermopower (orange triangles) as a function of surface coverage (in percents). We found that the average conductance actually increased with the number of surface molecules, but the thermopower decreased, thus eventually leading to a decrease in ZT .

The origin of this effect is the fact that the surface coverage induces two competing processes. On one hand, the addition of molecules bound to the surface adds conduction channels (i.e. local resonances in the transmission function) and therefore increases the conductance. On the other hand, the presence of disorder tends to flatten the resonances on average, and as a result the thermopower, which is proportional to the derivative of the transmission function [4], and hence becomes smaller as the transmission resonance becomes wider, is reduced. This competition is reflected in the opposite trends of G and S in the inset of Fig. 3. Since ZT is the product of the conductance which increases and the thermopower which decreases, it exhibits non-monotonic behavior.

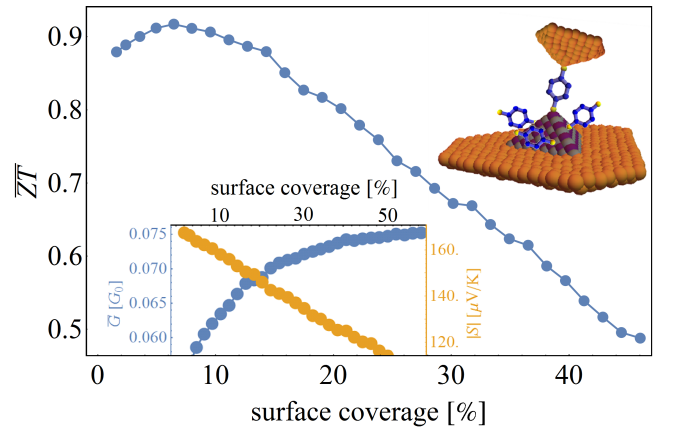


FIG. 3. ZT as a function of surface coverage (in percents) of molecules attached to the nanoparticle surface. Upper inset: schematic representation of the surface-attached molecules. Lower inset: average conductance (blue circles) and thermopower (orange triangles) as a function of number of surface molecules.

At room temperature it is possible that the electron motion across the junction will not be coherent and that

the electrons will dephase as they cross the molecule-NP interface. This may occur due to the interaction of electrons with the (soft) phonons of the NP, or due to vibrations in the position of the molecule with respect to the electrodes (but not due to interaction of electrons with the molecular vibrations, which are typically high-energy modes; such interactions were discussed in, e.g. [63]). If this is the case, the formulation presented above is invalid, as it describes coherent transport. To account for decoherence, we note that if the electron loses its phase on the molecule-NP interface, then the NP can, in fact, be considered as a semiconducting electrode. This results in an effective SC-molecule-metal junction, which can again be described using the Landauer formula, with the appropriate choice of self-energies.

To model the SC electrode, we recall that the imaginary part of the self-energy describes the electrode DOS. Similar to the wide-band approximation for the metallic electrode, we model the semiconducting electrode as constant outside the gap and zero in the gap. The imaginary part of the semiconducting self-energy can thus be written with the use of a heaviside step function Θ as $\text{Im}\Sigma_{SC} = \frac{\Gamma_B}{2} (\Theta(|E - \epsilon_c| - \frac{\Delta}{2}))$, and the real part of the self-energy determined via the Kramers-Kronig relation [27, 64]. In the numerical calculations given below, the step-function discontinuity is broadened by 0.01 eV, a value that can arise in realistic systems from lattice impurities and dislocations or thermal fluctuations.

In Fig. 4 we plot the (a) conductance, (b) thermopower, (c) thermal conductance and (d) ZT , for the hybrid SC-NP-molecule-metal junction (solid lines) as a function of ϵ_0 , with $\Gamma_B = 0.05$ eV, $\Gamma_T = 0.01$ eV, $\epsilon_c = -4.8$ eV, and $\Delta = 0.8$ eV. Looking at ZT , we find that the dephasing process in the NP does not substantially reduce the maximal ZT from the coherent case (the maximal value of Fig. 2). For comparison, the dashed lines of Fig. 4(a-d) show the same for $\Delta = 0$, i.e. a "standard" metal-molecule-metal (M-M-M) junction. The two most striking features of the comparison between the hybrid junction and the M-M-M junction are (i) the thermopower is substantially larger for the hybrid junction

and over a wider range of ϵ_0 , and (ii) ZT of the hybrid junction is roughly twice as large as that of the M-M-M junction.

The inset of Fig. 4(d) shows the inverse Lorenz number $\frac{L_0}{L}$ as a function of ϵ_0 for the hybrid junction (solid line) and M-M-M junction (dashed line). While a violation of the Wiedeman-Franz (WF) law $\frac{L_0}{L} \sim 1$ is observed for both types of junctions, the hybrid junction shows a much larger violation, which in fact determines the position of the maximal ZT , while for the M-M-M junction, the position of the maximal ZT is determined by the maximum of S .

Up till now, we considered a molecule which is weakly coupled to the electrodes. However, depending on the chemical moiety, the coupling between the molecule and the electrodes can be much larger (see, e.g. [9, 10, 59]). It is therefore of interest to see whether the increase in ZT in hybrid junctions compared to the M-M-M junctions is maintained also for strongly coupled molecules. In Fig. 4(e-h), the same as in Fig. 4(a-d) is plotted for a strongly coupled molecule, with $\Gamma_B = 0.5$ eV, $\Gamma_T = 0.1$ eV. Again, the two most striking differences between the hybrid junction and the M-M-M junction are the thermopower and ZT , which are even more profound for the strongly coupled junction. Due to the large value of the coupling, the transmission resonance of the M-M-M junction is very broad, and therefore the thermopower is very small. That, in addition with the fact that the WF law is obeyed (shown in the inset of Fig. 4(h), dashed line) results in a small $ZT \sim 10^{-2}$. In contrast, the hybrid junction (solid lines) shows only slight reduction of the thermopower (Fig. 4(f)), because although the molecular level is broadened due to the metallic lead, the band-edge of the SC electrode still introduces a sharp feature to the transmission function. Along with a violation of the WF law (inset of Fig. 4(h)), this leads to a relatively large $ZT \sim 1$. Surprisingly, ZT for the strongly-coupled hybrid junction displays larger ZT than the weakly-coupled junction, with large values of ZT for ϵ_0 well inside the SC band gap (as a result of the WF law violation inside the gap).

As was noted earlier, one of the advantages of the hybrid NP-molecule junctions is the ability to tune not the molecular orbitals, but the SC-NP band structure. With this in mind, in Fig. 5 we plot ZT for a constant value of the molecular orbital $\epsilon_0 = -5.2$ eV, as a function of the band-gap Δ (the band center is at $\epsilon_c = -4.8$ eV and $\Delta = 0$ corresponds to a M-M-M junction, see Fig. 1(a)), exploring the two cases of weakly coupled molecule (solid blue line) and strongly coupled molecule (dashed red line), as described above. For the weakly coupled molecule we see an increase of a factor 2 from

the M-M-M junction to the optimal band-gap. For the strongly coupled junction we find that ZT can rise as high as ~ 0.6 , with a four orders of magnitude increase in ZT compared to the M-M-M junctions. The inset shows S as a function of Δ , and both the weakly-coupled and strongly-coupled molecules exhibit orders-of-magnitude increase in S compared to the M-M-M junctions.

Finally, in Fig. 6, the temperature dependence of ZT is examined for the weakly-coupled hybrid molecular junction, evaluated for $\epsilon_0 = -5.2$ eV (corresponding to the maximum in ZT from Fig. 4(d)) (the rest of the pa-

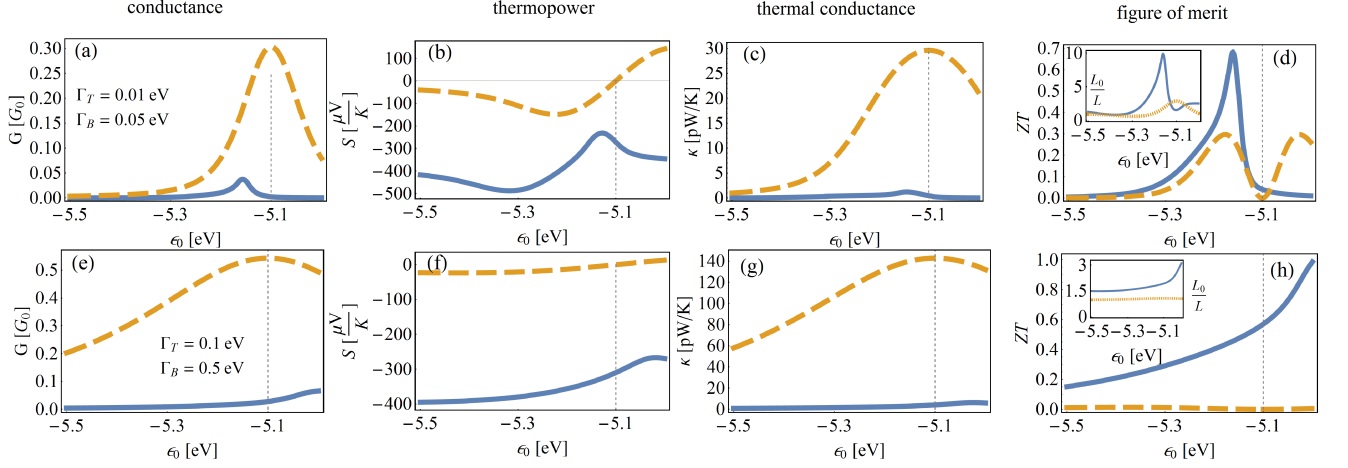


FIG. 4. (a) conductance, (b) thermopower, (c) thermal conductance and (d) ZT as a function of molecular orbital energy ϵ_0 , for a semiconductor-molecule-metal junction (solid lines) and a metal-molecule-metal junction (dashed lines), calculated for a weakly coupled molecule ($\Gamma_B = 0.05$ eV, $\Gamma_T = 0.01$ eV). Inset of (d): Inverse Lorenz number as a function of ϵ_0 . (e-h) same as (a-d), for a strongly coupled molecule ($\Gamma_B = 0.05$ eV, $\Gamma_T = 0.01$ eV).

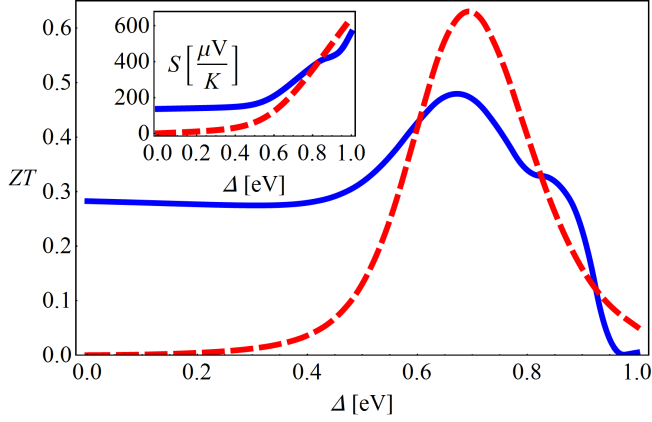


FIG. 5. ZT as a function of the SC NP band-gap Δ at constant molecular level $\epsilon_0 = -5.2$ eV, for weakly coupled (solid blue line) and strongly coupled (dashed red line) molecule. Inset: S as a function of Δ .

rameters are the same as in Fig. 4(a-d)). ZT is found to increase with temperature, exhibiting a maximum of $ZT \sim 2$ at $T \sim 450$ K, followed by a moderate decrease. This finding again implies that relatively large values of ZT persist in a broad range of parameters. In fact, in the inset of Fig. 5, we plot ZT calculated with an over-evaluated value of the phonon thermal conductance $\kappa_{phn} = 150$ pW/K, and we find that ZT reaches values of $ZT \sim 0.3$, which is still several orders of magnitude larger than the observed values.

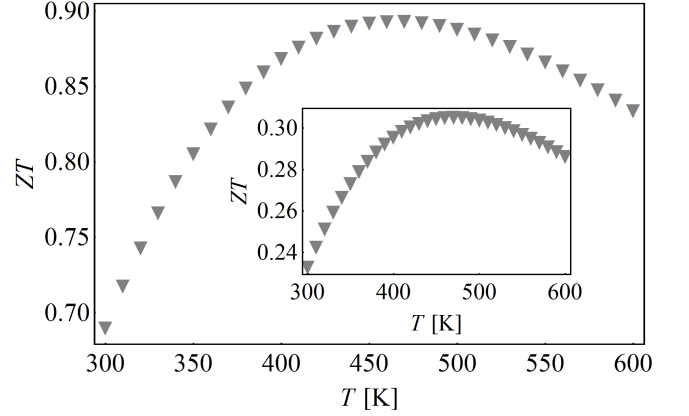


FIG. 6. Temperature dependence of ZT for $\epsilon_0 = -5.16$ eV. Inset: same, but with $\kappa_{phn} = 150$ pW/K.

SUMMARY AND CONCLUSIONS

In summary, we presented calculations of thermopower and thermoelectric FOM for a hybrid metal-single molecule- semiconducting nanoparticle-metal molecular junction. The presence of the SC-NP and the position of the molecular orbital close to the semiconducting band edge enhanced the particle-hole asymmetry required for efficient thermoelectric conversion. The resulting values of thermopower and ZT were much larger than those measured in experiments, and reach values as high as $S \sim 500$ $\mu\text{V/K}$ and $ZT \sim 1$ (an improvement of four orders of magnitude improvement over measured molecular junctions). We showed that this enhanced thermoelectric performance persists over a wide range of parameters and is robust against disorder in the form of

surface-attached molecules. We showed that decoherence at the molecule-nanoparticle boundary is not detrimental to the thermoelectric performance, and that large values of ZT persist up to high temperatures. Comparing hybrid SC-NP-molecule junctions to the more "standard" metal-molecule-metal junction, we found that for weakly-coupled molecules there is a factor ~ 2 increase in ZT and a factor ~ 4 in the thermopower. For strongly coupled molecules, the advantage of hybrid NP-molecule junctions is even more profound, with $2 - 4$ orders of magnitude increase in ZT and thermopower in hybrid junctions.

The model we presented here is a generic model, not aimed at any specific system. Nevertheless, our numerical parameters were taken from experimentally observed value, including the phononic contribution to the thermal conductance. This, along with the fact that enhanced thermoelectric performance was found for a wide range of molecular parameters and was robust against disorder, decoherence and high temperatures, strongly suggest that high values of thermopower can be reached in future experiments on molecule-nanoparticle junctions, which are promising candidates for nano-scale thermoelectric conversion.

ACKNOWLEDGMENTS

The authors acknowledge funding from the BGU-UM joint research initiative (Adelis Foundation).

* jdubi@bgu.ac.il

- [1] A. Aviram and M. A. Ratner, Chemical Physics Letters **29**, 277 (1974).
- [2] S. V. Aradhya and L. Venkataraman, Nat Nano **8**, 399 (2013).
- [3] M. Tsutsui and M. Taniguchi, Sensors **12**, 7259 (2012).
- [4] Y. Dubi and M. Di Ventra, Reviews of Modern Physics **83**, 131 (2011).
- [5] L. E. Bell, Science **321**, 1457 (2008).
- [6] X. Wang and E. Zhiming M. Wang, *Nanoscale Thermoelectrics* (Springer, 2014).
- [7] G. Mahan and J. Sofo, Proceedings of the National Academy of Sciences **93**, 7436 (1996).
- [8] P. Murphy, S. Mukerjee, and J. Moore, Phys. Rev. B **78**, 161406 (2008).
- [9] J. P. Bergfield and C. A. Stafford, Nano Letters **9**, 3072 (2009).
- [10] J. P. Bergfield, M. A. Solis, and C. A. Stafford, ACS Nano **4**, 5314 (2010), <http://dx.doi.org/10.1021/nn100490g>.
- [11] C. M. Finch, V. M. Garcia-Suarez, and C. J. Lambert, Phys. Rev. B **79**, 033405 (2009).
- [12] O. Karlström, H. Linke, G. Karlström, and A. Wacker, Phys. Rev. B **84**, 113415 (2011).
- [13] D. Nozaki, H. Sevinçli, W. Li, R. Gutiérrez, and G. Cuniberti, Physical Review B **81**, 235406 (2010).
- [14] R. Stadler and T. Markussen, The Journal of Chemical Physics **135**, 154109 (2011).
- [15] H. Nakamura, T. Ohto, T. Ishida, and Y. Asai, Journal of the American Chemical Society **135**, 16545 (2013).
- [16] J. Vacek, J. V. Chocholousova, I. G. Stara, I. Stary, and Y. Dubi, Nanoscale **7**, 8793 (2015).
- [17] J. Malen, P. Doak, K. Baheti, T. Tilley, A. Majumdar, and R. Segalman, Nano letters **9**, 3406 (2009).
- [18] J. Malen, P. Doak, K. Baheti, T. Tilley, R. Segalman, and A. Majumdar, Nano letters **9**, 1164 (2009).
- [19] J. Malen, S. Yee, A. Majumdar, and R. Segalman, Chemical Physics Letters **491**, 109 (2010).
- [20] P. Reddy, S. Jang, R. Segalman, and A. Majumdar, Science **315**, 1568 (2007).
- [21] J. R. Widawsky, P. Darancet, J. B. Neaton, and L. Venkataraman, Nano Letters **12**, 354 (2012).
- [22] J. R. Widawsky, W. Chen, H. Vazquez, T. Kim, R. Breslow, M. S. Hybertsen, and L. Venkataraman, Nano letters **13**, 2889 (2013).
- [23] W. B. Chang, C.-K. Mai, M. Kotiuga, J. B. Neaton, G. C. Bazan, and R. A. Segalman, Chemistry of Materials **26**, 7229 (2014), <http://dx.doi.org/10.1021/cm504254n>.
- [24] Y. Kim, W. Jeong, K. Kim, W. Lee, and P. Reddy, Nature nanotechnology **9**, 881 (2014).
- [25] J. Balachandran, P. Reddy, B. D. Dunietz, and V. Gavini, The Journal of Physical Chemistry Letters **3**, 1962 (2012).
- [26] S. K. Lee, T. Ohto, R. Yamada, and H. Tada, Nano letters **14**, 5276 (2014).
- [27] M. Di Ventra, *Electrical Transport in Nanoscale Systems* (Cambridge University Press, 2008).
- [28] E. Scheer and J. C. Cuevas, *Molecular electronics: an introduction to theory and experiment*, Vol. 1 (World Scientific, 2010).
- [29] C. Goupil, W. Seifert, K. Zabrocki, E. Müller, and G. J. Snyder, Entropy **13**, 1481 (2011).
- [30] C. B. Vining, Nature Materials **8**, 83 (2009).
- [31] W.-L. Ong, S. Majumdar, J. A. Malen, and A. J. McGaughey, The Journal of Physical Chemistry C **118**, 7288 (2014).
- [32] D. Segal, A. Nitzan, and P. Hänggi, The Journal of chemical physics **119**, 6840 (2003).
- [33] Z. Wang, J. A. Carter, A. Lagutchev, Y. K. Koh, N.-H. Seong, D. G. Cahill, and D. D. Dlott, Science **317**, 787 (2007).
- [34] S. Ballmann and H. B. Weber, New Journal of Physics **14**, 123028 (2012).
- [35] B. Capozzi, Q. Chen, P. Darancet, M. Kotiuga, M. Buzzeo, J. B. Neaton, C. Nuckolls, and L. Venkataraman, Nano Letters **14**, 1400 (2014), <http://pubs.acs.org/doi/pdf/10.1021/nl404459q>.
- [36] F. Prins, A. Barreiro, J. W. Ruitenbergh, J. S. Seldenthuis, N. Aliaga-Alcalde, L. M. K. Vandersypen, and H. S. J. van der Zant, Nano Letters **11**, 4607 (2011), <http://pubs.acs.org/doi/pdf/10.1021/nl202065x>.
- [37] V. I. Klimov, *Semiconductor and metal nanocrystals: synthesis and electronic and optical properties* (CRC Press, 2003).
- [38] U. Banin and O. Millo, Annual review of physical chemistry **54**, 465 (2003).
- [39] D. V. Talapin, J.-S. Lee, M. V. Kovalenko, and E. V. Shevchenko, Chemical Reviews **110**, 389 (2010), pMID: 19958036, <http://dx.doi.org/10.1021/cr900137k>.

- [40] J. Liao, L. Bernard, M. Langer, C. Schönenberger, and M. Calame, *Advanced Materials* **18**, 2444 (2006).
- [41] S. H. M. Jafri, T. Blom, K. Leifer, M. Strömme, H. Löfräs, A. Grigoriev, R. Ahuja, and K. Welch, *Nanotechnology* **21**, 435204 (2010).
- [42] W. Huang, G. Masuda, S. Maeda, H. Tanaka, and T. Ogawa, *Chemistry-a European Journal* **12**, 607 (2006).
- [43] B. Fainberg and T. Seideman, *physica status solidi (a)* **209**, 2433 (2012).
- [44] M. G. Reuter, T. Hansen, T. Seideman, and M. A. Ratner, *The Journal of Physical Chemistry A* **113**, 4665 (2009).
- [45] C. Delerue and M. Lannoo, *Nanostructures: theory and modelling* (Springer Science & Business Media, 2004).
- [46] G. Schmid, *Nanoparticles: from theory to application* (John Wiley & Sons, 2011).
- [47] J. G. Diaz, J. Planelles, G. W. Bryant, and J. Aizpurua, *The Journal of Physical Chemistry B* **108**, 17800 (2004), <http://dx.doi.org/10.1021/jp047658+>.
- [48] N. A. Hill and K. B. Whaley, *The Journal of chemical physics* **100**, 2831 (1994).
- [49] T. Li and G. Galli, *The Journal of Physical Chemistry C* **111**, 16192 (2007).
- [50] J. M. Azpiroz, J. M. Ugalde, and I. Infante, *Journal of Chemical Theory and Computation* **10**, 76 (2014).
- [51] Y. Meir, N. S. Wingreen, and P. A. Lee, *Phys. Rev. Lett.* **66**, 3048 (1991).
- [52] F. M. Souza, J. C. Egues, and A. P. Jauho, *Phys. Rev. B* **75**, 165303 (2007).
- [53] Y. Meir and N. S. Wingreen, *Phys. Rev. Lett.* **68**, 2512 (1992).
- [54] C. J. O. Verzijl, J. S. Seldenthuis, and J. M. Thijssen, *The Journal of Chemical Physics* **138**, 094102 (2013).
- [55] S. Datta, *Electronic Transport in Mesoscopic Systems* (Cambridge University Press, 1997).
- [56] U. Peskin, *Journal of Physics B: Atomic, Molecular and Optical Physics* **43**, 153001 (2010).
- [57] P. Khanna, K.-W. Jun, A. Gokarna, J.-O. Baeg, and S. I. Seok, *Materials Chemistry and Physics* **96**, 154 (2006).
- [58] C.-W. Wang, H.-G. Liu, X.-T. Bai, Q. Xue, X. Chen, Y.-I. Lee, J. Hao, and J. Jiang, *Crystal Growth & Design* **8**, 2660 (2008), <http://dx.doi.org/10.1021/cg070398b>.
- [59] M. Paulsson and S. Datta, *Phys. Rev. B* **67**, 241403 (2003).
- [60] J. Zhou, S. Samanta, C. Guo, J. Locklin, and B. Xu, *Nanoscale* **5**, 5715 (2013).
- [61] J. Zhou, G. Chen, and B. Xu, *The Journal of Physical Chemistry C* **114**, 8587 (2010).
- [62] I. Diez-Perez, J. Hihath, T. Hines, Z.-S. Wang, G. Zhou, K. Müllen, and N. Tao, *Nature nanotechnology* **6**, 226 (2011).
- [63] J. Ren, J.-X. Zhu, J. E. Gubernatis, C. Wang, and B. Li, *Phys. Rev. B* **85**, 155443 (2012).
- [64] G. D. Mahan, *Many-particle physics* (Springer, 2000).